Neuron, Vol. 37, 787–800, March 6, 2003, Copyright ©2003 by Cell Press

Functional Inactivation of a Fraction of Excitatory Synapses in Mice Deficient for the Active Zone Protein Bassoon

Wilko D. Altrock,[1,9] Susanne tom Dieck,[1,2,9] Maxim Sokolov,[1,9] Alexander C. Meyer,[3,9] Albrecht Sigler,[3] Cord Brakebusch,[4] Reinhard Fässler,[4] Karin Richter,[5] Tobias M. Boeckers,[1,6] Heidrun Potschka,[7] Claudia Brandt,[7] Wolfgang Löscher,[7] Dörte Grimberg,[1] Thomas Dresbach,[1] Anne Hempelmann,[1] Hadir Hassan,[1] Detlef Balschun,[1] Julietta U. Frey,[1] Johann H. Brandstätter,[2] Craig C. Garner,[8,*] Christian Rosenmund,[3] and Eckart D. Gundelfinger[1,*]

[1]Leibniz Institute for Neurobiology
39118 Magdeburg
[2]Max Planck Institute for Brain Research
Department of Neuroanatomy
60528 Frankfurt/M
[3]Max Planck Institute for Biophysical Chemistry
Department of Membrane Biophysics
37070 Göttingen
[4]Max Planck Institute for Biochemistry
Department of Molecular Medicine
82152 Martinsried
[5]Institute for Medical Neurobiology
Otto von Guericke University
39120 Magdeburg
[6]Institute for Anatomy
University of Münster
48149 Münster
[7]Department of Pharmacology,
Toxicology and Pharmacy
School of Veterinary Medicine
30559 Hanover
Germany
[8]Department of Psychiatry and Behavioral Science
Stanford University
Palo Alto, California 94304

Summary

Mutant mice lacking the central region of the presynaptic active zone protein Bassoon were generated to establish the role of this protein in the assembly and function of active zones as sites of synaptic vesicle docking and fusion. Our data show that the loss of Bassoon causes a reduction in normal synaptic transmission, which can be attributed to the inactivation of a significant fraction of glutamatergic synapses. At these synapses, vesicles are clustered and docked in normal numbers but are unable to fuse. Phenotypically, the loss of Bassoon causes spontaneous epileptic seizures. These data show that Bassoon is not essential for synapse formation but plays an essential role in the regulated neurotransmitter release from a subset of glutamatergic synapses.

*Correspondence: gundelfinger@ifn-magdeburg.de (E.D.G.), cgarner@stanford.edu (C.C.G.)
[9]These authors contributed equally to this work.

Introduction

At chemical synapses, neurotransmitter release is restricted to a specialized region of the presynaptic plasma membrane, the active zone. Regulated release of transmitter is accomplished by a spatially and temporally tightly controlled series of membrane trafficking events, commonly referred to as the synaptic vesicle (SV) cycle, which takes place in the vicinity of the active zone (Südhof, 1995, 2000). During this cycle, transmitter-filled SVs dock at the active zone and become fusion competent in a series of priming steps. In response to activity-triggered Ca^{2+} influx, primed SVs release their content into the synaptic cleft and are rapidly recycled.

At the ultrastructural level, the active zone is characterized by an electron-dense structure that is tightly associated with the plasma membrane. This presynaptic dense projection or cytomatrix at the active zone (CAZ) is exactly aligned with the postsynaptic neuroreception apparatus defined by the postsynaptic density (Peters et al., 1991; Dresbach et al., 2001). The CAZ extends from the presynaptic plasma membrane into the bouton, where it is associated with a pool of SVs.

Molecular components of the CAZ, including the CAZ-specific proteins Munc13, RIM, CAST, Bassoon, and Piccolo, are thought to define and organize the site of transmitter release. Munc13 isoforms are involved in SV priming and are major targets for the second messenger diacylglycerol in regulating transmitter release (Rhee et al., 2002; Rosenmund et al., 2002). RIMs, which physically and functionally interact with Munc13 in making SVs fusion competent (Betz et al., 2001; Schoch et al., 2002), are effectors of the small GTPase Rab3a. CAST is a structural CAZ protein that interacts with RIM and Munc13 (Ohtsuka et al., 2002). Bassoon and Piccolo/Aczonin are structurally related CAZ proteins present at both excitatory and inhibitory synapses (tom Dieck et al., 1998; Richter et al., 1999; Wang et al., 1999; Fenster et al., 2000). During synaptogenesis, Bassoon and Piccolo are among the earliest components to appear at the newly formed site of neurotransmitter release (Vardinon-Friedman et al., 2000; Zhai et al., 2001), suggesting that they are important in the assembly of functional active zones (Garner et al., 2002).

Piccolo and Bassoon share regions of high sequence similarity, which include two double zinc finger motifs in the N-terminal region and three coiled-coil domains in the central part of the molecules (Fenster et al., 2000). Piccolo additionally harbors a PDZ and one or two C2 domains near the C terminus. RIMs share structural similarities with Piccolo, as they contain one N-terminal zinc finger, a PDZ, and two C-terminal C2 domains (Wang et al., 1997). Interestingly, whereas RIMs are present in both *C. elegans* and *Drosophila* (Wang et al., 1997), homologs of Bassoon and Piccolo appear to be de novo developments of vertebrates.

Ultrastructural morphometric studies at the active zone of both conventional synapses and of ribbon synapses in the retina indicate a precise orientation of Bassoon and Piccolo (Brandstätter et al., 1999; Zhang et al., 2000; Dick et al., 2001). These large extended cytoskeletal-like proteins appear to span the entire CAZ from the presynaptic plasma membrane deep into the presynaptic space (Brodin et al., 1997; Dresbach et al., 2001). Therefore, it is conceivable that the two proteins are involved in the assembly of the presynaptic apparatus and/or in the organization of various steps of the SV cycle. To directly test this hypothesis, we have produced a mouse mutant lacking the central exons of the *Bassoon* (*Bsn*) gene. Our data show that this central region is critical for anchoring Bassoon to the CAZ. Although mutant hippocampal synapses look structurally normal, a fraction of them is inactive.

Results

Transcripts and Proteins in *Bsn* Mutant Mice

To disrupt the *Bsn* gene, a mouse mutant was generated, in which parts of exon 4 and the entire exon 5 were replaced by a *lacZ/neomycin* cassette (Figure 1A). Mutant mice were genotyped by Southern blotting (Figure 1B) or PCR (not shown). By Northern analysis of brain RNA, wild-type (WT) transcripts were not detectable in homozygous (−/−) mutants (Figure 1D). Instead, mutants synthesize two transcripts of 6 and 9 kb. The 6 kb transcript represents the expected bicistronic mRNA encoding an N-terminal fragment of Bassoon and β-galactosidase. The 9 kb transcript results from joining exons 3 and 6 of the *Bsn* gene (Figure 1C) as confirmed by RT-PCR (data not shown).

To assess whether Bassoon remnants were still expressed in mutant mice, antibodies against different regions of Bassoon were used to probe immunoblots of brain extracts. As expected, no immunoreactive bands were detected with antibodies against the central portion of Bassoon (data not shown). In contrast, antisera against the N terminus of Bassoon detected a 180 kDa band on immunoblots (Figure 1F). This mutant Bassoon variant is not found in WT mice, lacks the central region encoded by exons 4 and 5 (BsnΔEx4/5), and appears to be translated from the 9 kb transcript (Figure 1F). The deletion removes amino acids 505 to 2889, i.e., the C-terminal half of the second zinc finger to a region N-terminal of the third coiled-coil domain of WT Bassoon (Figure 1E). The predicted 67 kDa N-terminal Bassoon fragment encoded by the 6 kb transcript was not detected on immunoblots (Figure 1F). However, the β-galactosidase encoded by the same transcript is synthesized in both homozygous and heterozygous mutant mice with a distribution in the brain similar to that of WT *Bsn* transcripts (data not shown). We therefore assume that the 67 kDa fragment is rapidly degraded after synthesis.

The Core Region of Bassoon Is Essential for CAZ Association

To examine if BsnΔEx4/5 can still associate with the CAZ, we prepared synaptic junction membranes from WT and −/− mice and assayed individual fractions for the presence of Bassoon immunoreactivity (IR). Whereas the 420 kD WT Bassoon copurifies with synaptic junctions, BsnΔEx4/5 is not enriched in this fraction (Figure 2A). Significant amounts of the 180 kDa protein are found in the cytoplasmic fraction (lane 2) and in the supernatant of lysed synaptosomes (lane 5), indicating that BsnΔEx4/5 does not tightly associate with the synaptic cytomatrix.

Primary cultures from hippocampal neurons of newborn WT and −/− mice were prepared to further assess the synaptic localization of BsnΔEx4/5. After 14 days in vitro (div), cultures were fixed with methanol, which releases soluble but not cytoskeletal proteins, and doubly immunostained with antibodies against the N-terminal region of Bassoon and the dendritic marker MAP2 (Figure 2C). While WT Bassoon is exquisitely localized in puncta along dendritic structures (Figure 2Ca), much less Bassoon IR is detectable along dendrites of −/− mutants (Figure 2Cb). Moreover, WT Bassoon is colocalized at many synapses with Piccolo (Figure 2Cc), whereas BsnΔEx4/5 protein is diffusely distributed, and its localization does not overlap with Piccolo in formaldehyde-fixed primary cultures (Figure 2Cd). Together the biochemical and immunocytochemical data indicate that BsnΔEx4/5 is clearly less efficiently anchored to the CAZ than WT Bassoon.

Loss of Bassoon Causes Increased Piccolo Levels

The absence of WT Bassoon did not affect the synaptic association of the CAZ components Piccolo, RIM, and Munc13-1 when analyzed by biochemical copurification with synaptic junctions from WT and −/− mice. While Piccolo behaves like WT Bassoon, a fraction of RIM and Munc13-1 always partitions into the soluble fractions, i.e., crude and synaptosomal cytoplasm (Figure 2A). We also tested whether deletion of the core region of Bassoon affects the abundance of the other CAZ components. No significant changes were found for RIM and Munc13, but Piccolo levels were upregulated 1.4-fold (Figure 2B).

Moreover, the colocalization of Piccolo and RIM IRs along dendritic profiles of mutant primary neurons (Figure 2Ce) indicates that the synaptic localization of these CAZ proteins is not affected by the absence of functional Bassoon. In addition, the presence of postsynaptic elements is indicated by colocalization with ProSAP1/Shank2 (Figure 2Cf). Normal localization of Piccolo in *Bsn*$^{-/-}$ mutants is also confirmed by immunogold labeling of brain synapses in situ (Figure 2E). These data suggest that neither the localization nor the synaptic association of other known CAZ proteins were adversely affected by the absence of WT Bassoon.

Viability and Synaptic Structure of *Bsn* Mutant Mice

Homozygous *Bsn* mutants are viable and appear normal at birth. While WT and heterozygotes survived normally, ~50% of −/− mutants died during the first 6 months, displaying the typical posture of animals that have died from epileptic seizures. No abnormalities in brain architecture were observed in *Bsn* mutants (data not shown).

Also at the ultrastructural level, no obvious differences were detected at synapses of various brain regions, including hippocampus (Figure 2D) and cerebellum (data not shown). A quantitative assessment of ultra-

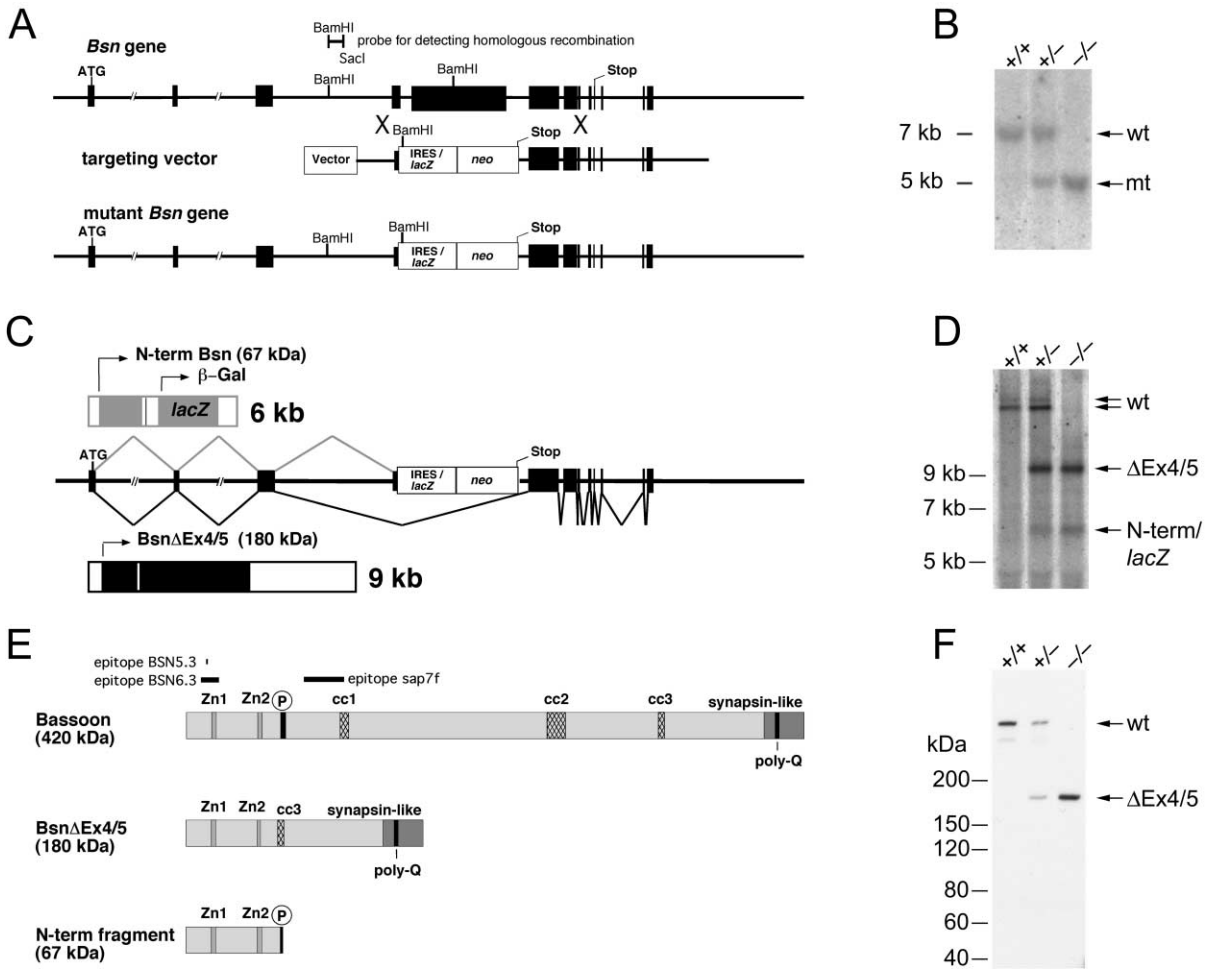

Figure 1. Targeted Disruption of the *Bsn* Gene and Analysis of Transcript and Protein Expression in *Bsn* Mutant Mice

(A) Maps of the *Bsn* gene, the targeting vector, and the resulting mutant gene, indicating the replacement of part of exon 4 and the entire exon 5 by an internal ribosomal entry site (IRES)-containing *lacZ/neo* cassette (black boxes represent exons). The BamHI/SacI fragment used as a probe and BamHI restriction sites used to detect homologous recombination in ES cells and to genotype mice by Southern blots are indicated.

(B) Southern blot analysis of BamHI-digested genomic DNA of WT (+/+), heterozygous (+/−), and homozygous mutant (−/−) mice.

(C) Alternative splicing of the mutant allele results in two transcripts. The 6 kb transcript encodes the N-terminal 67 kDa fragment of Bassoon and β-galactosidase. In-frame splicing from exon 3 to exon 6 gives rise to a 9 kb transcript encoding BsnΔEx4/5.

(D) Northern analysis of brain RNA reveals two transcripts (>13 kb) in WT mice, the two transcripts depicted in (C) in −/− mutants, and all four transcripts in +/− mice. Blots were hybridized with an exon 2 probe.

(E) Schematic representation of Bassoon proteins derived from WT and mutant transcripts. In BsnΔEx4/5 aa 505 to 2889 are missing. The predicted 67 kDa N-terminal fragment ends within the repetitive potential phosphorylation sites for proline-directed protein kinases (P). Zn, zinc finger; cc, coiled-coil region; poly-Q, poly-glutamine stretch. The locations of epitopes for antibodies used in this study are indicated.

(F) Immunoblot analysis of 10 μg/lane of brain homogenate from +/+, +/−, and −/− mice. Antibody BSN5.3 detects WT Bassoon in +/+ and +/− animals and BsnΔEx4/5 in +/− and −/− mice; the 67 kDa N-terminal fragment is not detectable.

structural parameters, similar to those applied to study RIM1α knockout mice (Schoch et al., 2002), was performed for synapses of the *stratum radiatum* of the hippocampal CA1 region. Neither synapse density nor parameters defining presynaptic nerve terminals, e.g., extension of the active zone, number of docked vesicles, SV density in the vicinity to the active zone, are significantly altered in −/− as compared to WT mice (Table 1).

Electrophysiological Characterization of Hippocampal Synapses

To study the function of Bassoon in synaptic transmission, basic electrophysiological properties of $Bsn^{-/-}$ mutants and their WT littermates were evaluated in acute hippocampal slices using extracellular and whole-cell patch-clamp recordings from CA1 pyramidal cells. Whole-cell recordings from −/− mice displayed a shift of input-output properties expressed as a significantly reduced excitability over a broad range of stimulation intensities (Figure 3Ab). Extracellular recordings showed the same trend but did not reach the level of statistical significance (Figure 3Aa). Next, we examined by evaluating the paired-pulse characteristics of CA1 synapses whether the initial release probability was affected. Depending on the initial release probability, synapses show a characteristic interpulse interval (IPI)-dependent de-

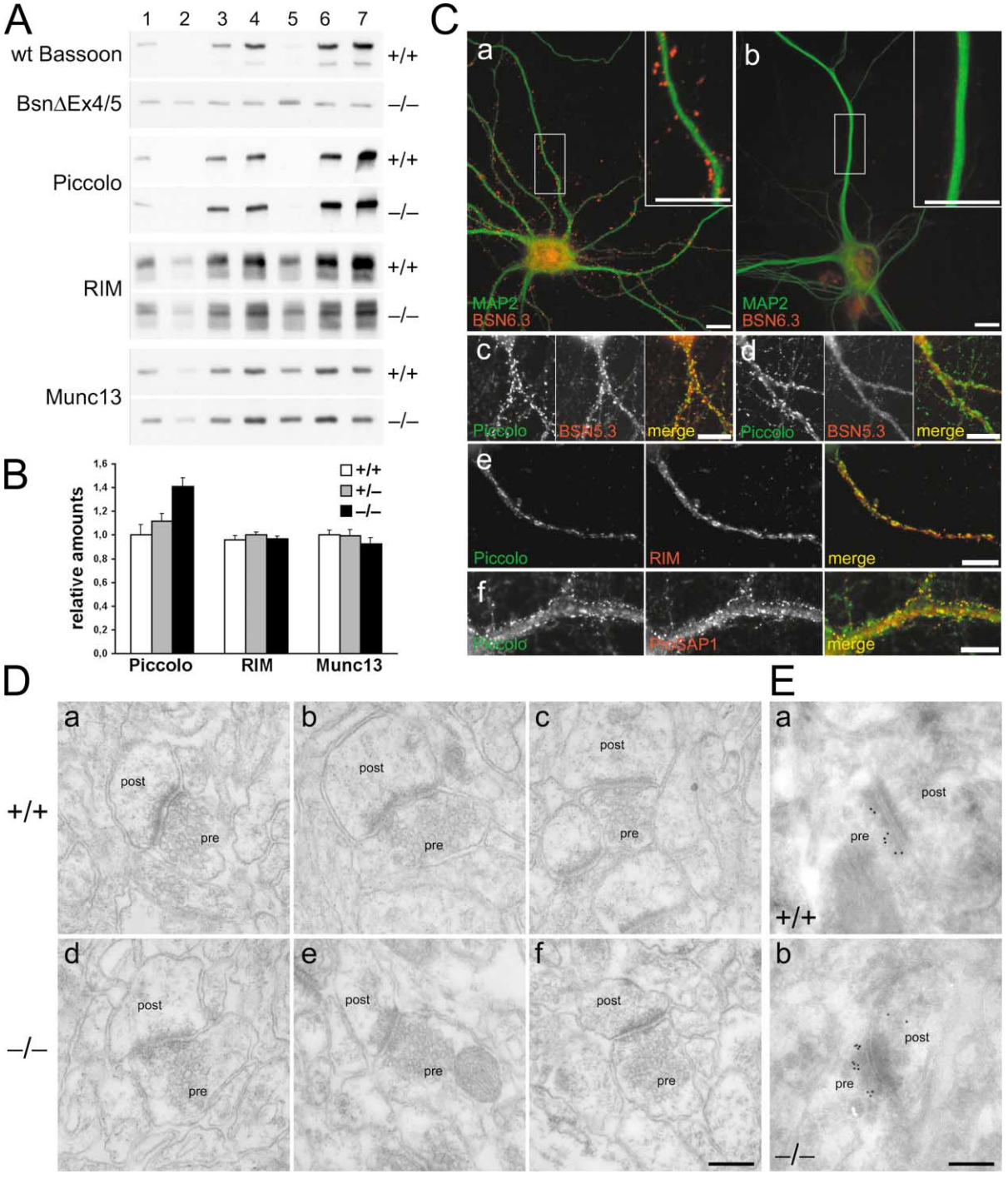

Figure 2. Expression and Synaptic Localization of CAZ Proteins in *Bsn* Mutant Mice

(A) Partitioning of CAZ proteins in synaptic membrane preparations from brains of WT and −/− mice. Immunoblots (10 μg protein/lane) of postnuclear supernatant S1 (lanes 1), cytoplasm S2 (2), crude membranes P2 (3), synaptosomes (4), synaptosomal cytoplasm S3 (5), synaptosomal membranes P3 (6), and synaptic junction plasma membranes (7) were developed with antibodies against Bassoon (BSN5.3), Piccolo, RIMs, and Munc13s. Note the presence of BsnΔEx4/5 in soluble fractions (lanes 2 and 5) in mutants.

(B) Piccolo levels are upregulated in −/− mice. Densitometric evaluation of Piccolo, RIM, and Munc13 immunoreactivities on Western blots of brain homogenates (10 μg protein/lane) from +/+, +/−, and −/− mice. Normalized to the WT signal of each preparation, the upregulation of Piccolo is 1.41 ± 0.07-fold in −/− mutants. Eight animals (2–5 months old) in six independent experiments were evaluated.

(C) Localization of CAZ proteins in primary hippocampal neurons of WT (Ca and Cc) and −/− mutants (Cb and Cd–Cf) at 14 div. The antiserum BSN6.3 yields a typical synaptic staining (red) along MAP2-positive dendrites (green) in methanol-fixed WT neurons (Ca). Punctate BSN6.3 staining is strongly reduced and sometimes completely absent in neurons from −/− mice (Cb). Piccolo IR and BSN5.3 IR largely colocalize in formaldehyde-fixed WT (Cc) but not in −/− neurons (Cd). Piccolo and RIM are codistributed in −/− neurons (Ce). Many of the Piccolo

Table 1. Morphometric Analysis of Synapses in the Stratum Radiatum of the Hippocampal CA1 Region of WT and −/− *Bsn* Mutants

Parameter	Wild-Type	−/− Mutants
Synapse density (per 100 μm²)[a]	56.7 ± 11	48.9 ± 3.2
SV density in the proximal zone (per μm²)[b]	222 ± 58	193 ± 53
Extension of the active zone (nm)[c]	248 ± 76	283 ± 95
Docked SVs (per μm)[d]	20.7 ± 7.1	17.4 ± 6.0

[a] Determined as number of postsynaptic densities (PSDs) per area from 117 and 119 randomly selected low-magnification electron micrographs from five WT and five −/− animals, respectively.
[b] Determined as number of SVs inside a semicircle around the active zone.
[c] Determined as the extension of the PSD.
[d] Defined as SVs, the centers of which lie within 50 nm distance from the presynaptic plasma membrane (Schoch et al., 2002).
[b–d] Data were obtained from high-magnification micrographs of synapses from three WT (n = 100) and three −/− animals (n = 80). The origins of micrographs were blinded for the observer. Data are presented as mean ± SD.

pression or facilitation of the synaptic response to the second stimulus (Zucker, 1989). Over an IPI range from 10 to 500 ms, WT and −/− mice showed no significant differences in their paired-pulse responses (Figure 3Ba). The same paradigm was employed to test inhibitory responses after pharmacological blockade of excitatory synaptic transmission. Again, WT and −/− mice displayed similar paired-pulse properties (Figure 3Bb). Finally, we tested whether the absence of Bassoon has consequences on synaptic depression induced by long trains of low-frequency stimulation (LFS, 900 pairs with 50 ms IPIs at 2 Hz). Homozygous mutants displayed a significantly weaker synaptic depression during stimulus application than WT mice, whereas long-term depression was unaffected (Figure 3C).

Characterization of Autaptic Hippocampal Primary Cultures

For a more detailed analysis of the synaptic phenotype, we performed patch-clamp recording of individual hippocampal neurons grown on microisland beds of glial cells. These cultures, which form recurrent "autaptic" synapses onto themselves, allow the simultaneous measurement of various release modes originating from the same synapse population. The analysis was focused on excitatory neurons, which represent the large majority of cells in this culture. We systematically analyzed *Bsn*$^{-/-}$ neurons 12–21 days after plating and compared them to control cells from WT littermates. Mutants displayed apparently normal basic electrophysiological behavior, including robust synaptic responses and normal mEPSC amplitudes. Mean mEPSC amplitude and charge showed no significant differences between mutant and WT cells, and mEPSC amplitude distributions superimposed nicely (Figure 4F), as did their mean (+/+: 15.6 ± 3.1 pA, 58 ± 11 fC, n = 4; −/−: 17.5 ± 3.5 pA, 62 ± 12 fC, n = 7). However, on average, both the size of the readily releasable SV pool (RRP) and the mean EPSC amplitude was reduced to about half of that of WT littermates (Figures 4A–4C). The RRP was quantified by integrating the transient inward current component of the response induced by a 4 s application of external solution that was 500 mOsm hypertonic (Rosenmund and Stevens, 1996). Mutants showed an average RRP of 481 ± 91 pC (corresponding to ~7700 vesicles, n = 30), while WT littermates had a RRP of 915 ± 168 pC (~15900 vesicles, n = 30, p = 0.025). Wild-type cells had an average EPSC amplitude of 6.9 ± 1.6 nA (~1030 vesicles, n = 27) compared to 3.7 ± 0.6 nA (~460 vesicles, n = 33, p = 0.05) of −/− cells. From the average EPSC charge and the RRP charge, we calculated the mean vesicular release probability as 5.4% ± 0.5% in WT and 7.1% ± 0.9% in −/− mice (p = 0.094; Figure 4D). This indicates that SVs that reach fusion competence have similar release probabilities and that the reduced EPSC amplitude is due to a reduced number of fusion-competent SVs. To determine whether this is due to less active release sites or less fusion-competent SVs per active zone, we measured the release probabilities of active zones by analysis of MK-801-dependent block of NMDA EPSCs (Rosenmund et al., 1993). The successive block rate of synaptic NMDA currents did not differ between WT and −/− mice (Figure 4E), indicating that the synaptic release probability is unaltered.

The reduced RRP size may reflect an impaired refilling with fusion-competent SVs. To test this, we applied pulses of hypertonic solution and measured how much of the evoked EPSC and the total pool had recovered 3 and 3.5 s after the end of the first pulse, respectively. For both WT and mutant groups, a recovery of the RRP to ~60% of the initial size (Figure 4G) and to ~30% of the initial evoked EPSC size (Figure 4J) was observed, indicating that lack of WT Bassoon has no effect on the kinetics of RRP refilling.

Consistent with the unchanged synaptic release probability, time courses during brief trains of stimulation (50 EPSCs at 10 Hz or 5 EPSCs at 50 Hz) were nearly identical for WT and −/− neurons (Figures 4H and 4I), suggesting that reduction of the RRP had no effect on short-term plasticity.

immunoreactive puncta colocalize with ProSAP1 (Cf), a postsynaptic marker of excitatory neurons, indicating the proper alignment of synapses in mutant cultures. Scale bars, 10 μm.
(D) Ultrastructure of synapses of the hippocampal CA1 region. The ultrastructural appearance of excitatory synapses is similar in WT (Da–Dc) and −/− mice (Dd–Df).
(E) Localization of Piccolo in the CAZ assessed with immunogold-labeled antibodies in WT (Ea) and −/− animals (Eb). Scale bar in (D) and (E), 200 nm.

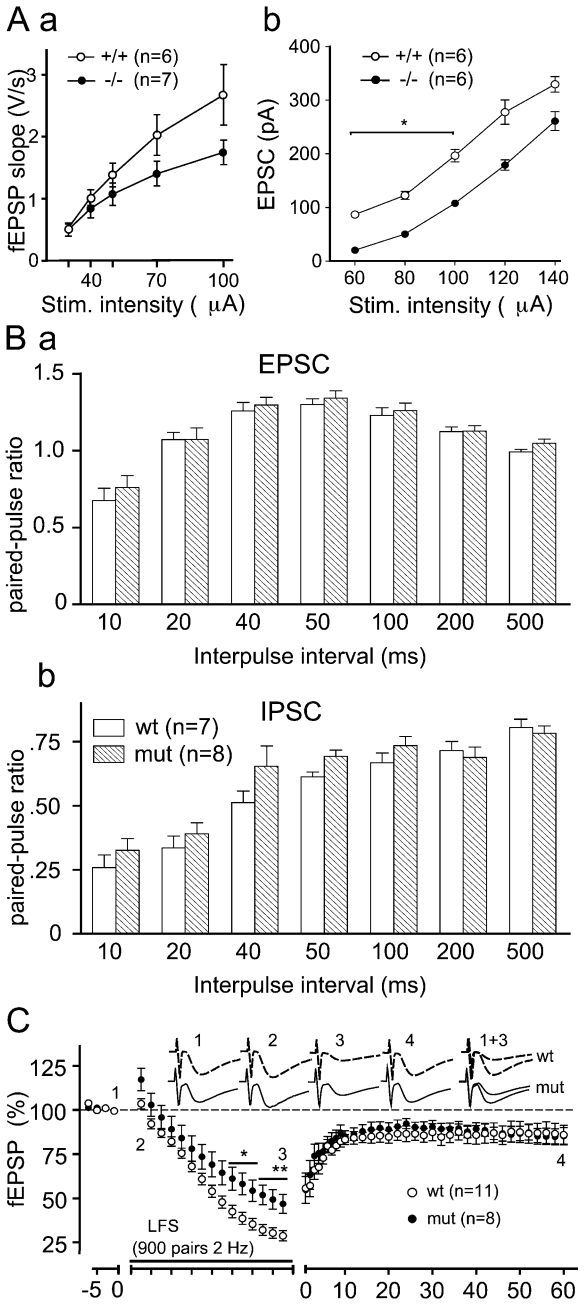

Figure 3. Electrophysiological Characterization of CA1 Synapses in WT and −/− Mice

(A) Dependence of fEPSP slope (Aa) and EPSC amplitude (Ab) on stimulus intensity. Homozygous mutants have a lower excitability, as particularly supported by the significantly lower values obtained in patch-clamp recordings (Ab) (*$p < 0.05$; ANOVA). Extracellular recordings (Aa) show the same trend.

(B) The paired-pulse ratio for EPSCs (Ba) and IPSCs (Bb) at different IPIs is indistinguishable between WT and mutants.

(C) −/− mice display a decreased synaptic fatigue during LTD-inducing LFS (900 stimulus pairs at 2 Hz; 50 ms IPI) in the presence of CPP to block NMDA receptors. Each point represents the average of 60 traces (*$p < 0.05$; **$p < 0.01$; Mann-Whitney U test). Insets show representative responses of individual experiments from WT (broken line) and −/− mice (solid line). Each trace represents ten averaged consecutive responses taken at the time points indicated by the numbers on the graph. Note the smaller reduction of fEPSP slope after LFS stimulation in the mutant as compared to WT mice (traces 1 + 3). All data are represented as mean ± SEM. The numbers in brackets represent sample sizes.

As a further control, experiments were performed to exclude that the sensitivity of mutant neurons to presynaptically released glutamate is reduced due to impaired postsynaptic AMPA receptor function. We exogenously applied the AMPA receptor agonist kainate (10 μM) to age-matched WT and mutant neurons and quantified the whole-cell inward current as a measure for relative AMPA receptor activity. Consistent with the finding that the mEPSC amplitude was unchanged, these responses were similar between WT (280 ± 77 pA, n = 7) and −/− neurons (302 ± 72 pA, n = 6).

From these data we can conclude that loss of WT Bassoon leads to a significant reduction of the total number of fusion-competent SVs, without affecting significantly quantal size, vesicular or synaptic release probabilities, vesicular refilling kinetics, or short-term plasticity. The simplest explanation for this observation is that the synapses monitored in our experiments are functionally indistinguishable from their WT counterparts but that in Bassoon-deficient neurons the number of actively releasing active zones/synapses is reduced.

We therefore performed a detailed analysis to quantify the total number of synapses and to test for impaired synapse formation in the mutants. Individual autaptic cells were immunostained for synapses with synaptophysin and for dendrites with MAP2 antibodies (Figure 5A). In WT and mutant cells, the average dendritic area was similar (Figure 5B; +/+: 1203 ± 102 μm^2, n = 18; −/−: 1246 ± 68 μm^2, n = 33). The corresponding total number of synapses (+/+: 641 ± 98, n = 18; −/−: 627 ± 72, n = 33) and the calculated density of synapses per dendritic area (Figure 5C; +/+: 0.54 ± 0.08 μm^{-2}, n = 18; −/−: 0.51 ± 0.05 μm^{-2}, n = 33) were also unchanged. This indicates that the loss of Bassoon does not impair the overall development of dendrites and synapses. Thus, as in the mutant functional synapses are WT-like and numbers of formed synapses are identical, it can be concluded that the reduction in evoked transmission should result from more inactive synapses in *Bsn*$^{-/-}$ mice.

The fraction of active and silent synapses was determined, blinded for the examiner, in a separate group of experiments. We directly compared synaptic structures and their release activity by performing dye labeling of active synapses combined with immunohistochemical detection of synaptic marker molecules. Exocytotic activity was detected by styryl dye FM1-43 uptake and release. The dye was loaded in active synapses during a brief application of a depolarizing high K^+ solution and unloaded 3 min later with a second high K^+ pulse. Active synapses were identified by the uptake of FM dye and the subsequent decrement of fluorescence in response to the first and second stimulus, respectively. Immediately after, cells were fixed and immunostained for synaptophysin and/or Piccolo to assess the total number of synapses and their localization.

These data sets were compared to each other by image overlay to determine the fraction of active syn-

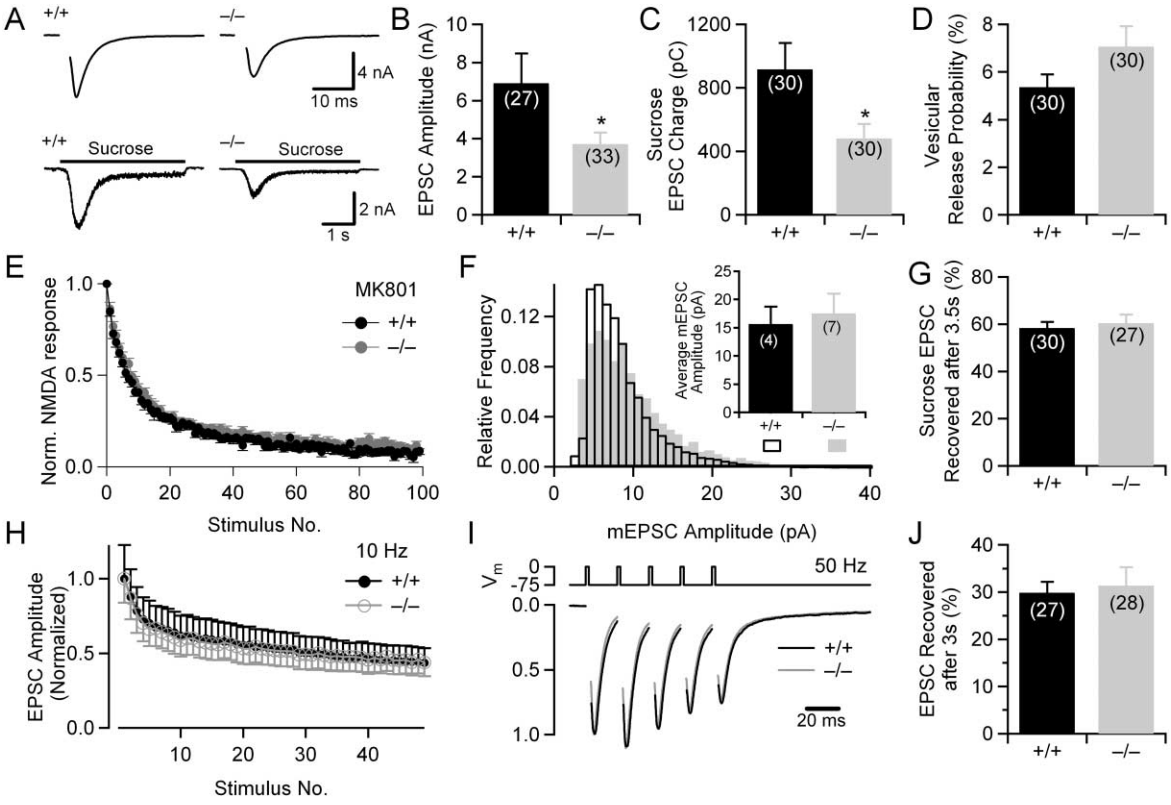

Figure 4. *Bsn*-Deficient Neurons Have a Reduced Number of Fusion-Competent SVs and Show Decreased Evoked Synaptic Responses

(A) Typical EPSC from a WT (left) and a −/− (right) excitatory neuron (upper row, stimulus artifact-blanked). Lower row: exemplary responses to 4 s application of 500 mOsm hypertonic external sucrose solution to quantify the total RRP. Holding potential was −75mV.

(B) Mean EPSC amplitudes for WT and −/− neurons (numbers in brackets indicate number of cells).

(C) Average RRP size estimate from hypertonic stimulation.

(D) Average vesicular release probability calculated as EPSC charge/charge of sucrose response.

(E) Comparison of release probabilities per active zone, assayed by measuring the successive decrease of NMDA current in the presence of MK-801.

(F) Averaged normalized histograms of mEPSC distributions of WT and −/− neurons. Inset: average mean of the distributions.

(G) Refilling kinetics of the RRP as estimated from paired-pulse sucrose experiments. The plot shows mean percentage recovery of the RRP within a 3 s IPI.

(H) Time course normalized EPSC amplitudes during a 10 Hz train (5 s). Average of 27 (+/+, black) and 33 (−/−, gray) cells.

(I) Superimposed EPSCs from WT and mutants during five successive responses evoked by brief depolarization at 50 Hz. The responses were normalized to the first EPSC amplitude. (stimulus artifact-blanked, +/+: n = 31; −/−: n = 32).

(J) Recovery of the evoked EPSC after total pool depletion with hypertonic solution.

apses (Figure 5E). First, we manually counted the amount of structures that releases FM but were not associated with synaptophysin. In both groups, they were in the range of 15% (+/+: 14% ± 2%, n = 1978 in 9 cells; −/−: 18% ± 2%, n = 4779 in 16 cells). These structures most likely do not represent synapses. Second, to determine the fraction of synaptic structures that are release inactive, we counted synaptic structures that did not colocalize with release activity (Figure 5D). While in WT cells 18% ± 3% (n = 2083, 9 cells) were inactive, the −/− neurons had twice as many release-inactive synapses (36% ± 2%, n = 6262, 16 cells; $p < 0.01$).

Next, we performed a careful pair-wise or triple-staining immunocytochemical analysis of the presence of other pre- and postsynaptic marker molecules at autapses of WT and −/− cultures (Figures 5F–5H). Analyzed molecules include presynaptic (Piccolo, synaptophysin, synaptobrevin/VAMP) and postsynaptic proteins (ProSAP1, NMDA receptor). In WT cells, the overlap of each pair of these markers was about 90%. Consistently, in WT neurons, 94% ± 1.4% of Bassoon-positive sites also are stained with Piccolo antibodies (n = 1016; five cells), and vice versa, 89% ± 3.8% of Piccolo-positive sites also carry Bassoon (n = 1126; five cells). Virtually no differences in the colocalization ratios of all tested molecules were observed between WT and −/− cultures (Figure 5F). This indicates that the lack of release activity at autapses is not correlated with loss of Piccolo or with the alignment to postsynaptic specializations. Altogether this set of experiments shows that the number of active synapses as detectable by FM cycling is significantly reduced in mutant neurons. This independently confirms the finding from the electrophysiological data that fewer synapses are releasing transmitter in mutants, although the degree of reduction in the electrophysiologically measured evoked responses was larger than the fraction of inactive synapses observed in the imaging experiments.

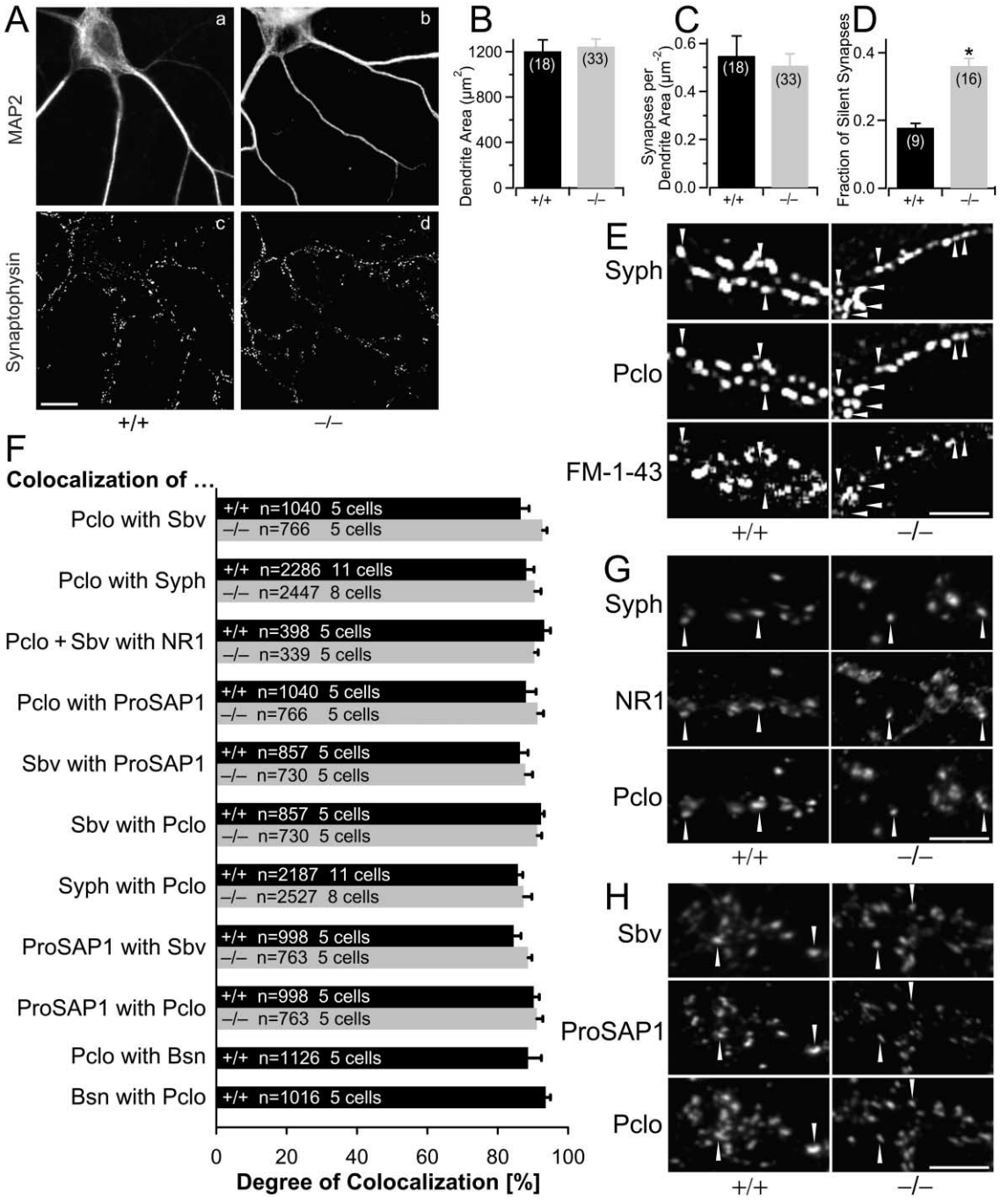

Figure 5. Structural and Functional Assessment of Synapses in Microisland Cultures from WT and −/− Mice

(A) Immunostains of autaptic neurons. (Aa and Ab) Staining for the dendritic marker MAP2 to assess the size of WT and −/− neurons; (Ac and Ad) staining of the same culture for synaptophysin (Syph) to assess the number of synapses.

(B) Average dendrite area of WT and −/− neurons determined from the indicated number of neurons.

(C) Density of synapses on dendrites measured as number of Syph-positive spots per μm^2 of dendrite.

(D) Percentage of inactive synapses determined as fraction of Syph-positive puncta not colocalized with FM1-43 cycling sites (defined by FM dye uptake and release in response to the first and second high K^+ pulse, respectively).

(E) Examples of differential FM1-43 uptake/release aligned with immunostains for Syph and Piccolo (Pclo) for WT (+/+) and mutant neurons. Arrowheads indicate Syph- and Piccolo-positive but FM1-43-negative spots.

(F) Colocalization of pairs or triplets of synaptic markers in WT and mutant autaptic cultures. Bars (black, WT; gray, mutant) represent the proportion of immunopositive spots of a given antigen (or pair of antigens) colocalizing with another antigen. Proteins included in the analysis are Piccolo (Pclo), synaptobrevin/VAMP (Sbv), synaptophysin (Syph), NR1 NMDA receptor subunit (NR1), ProSAP1/Shank2 (ProSAP1), and in WT cells, Bassoon (Bsn).

(G and H) Examples of colocalizations after triple immunofluorescence labeling for indicated proteins. Here, arrowheads depict examples of colocalization. Scale bar in (A), 10 μm. Scale bars in (E), (G), and (H), 5 μm. Error bars represent standard errors.

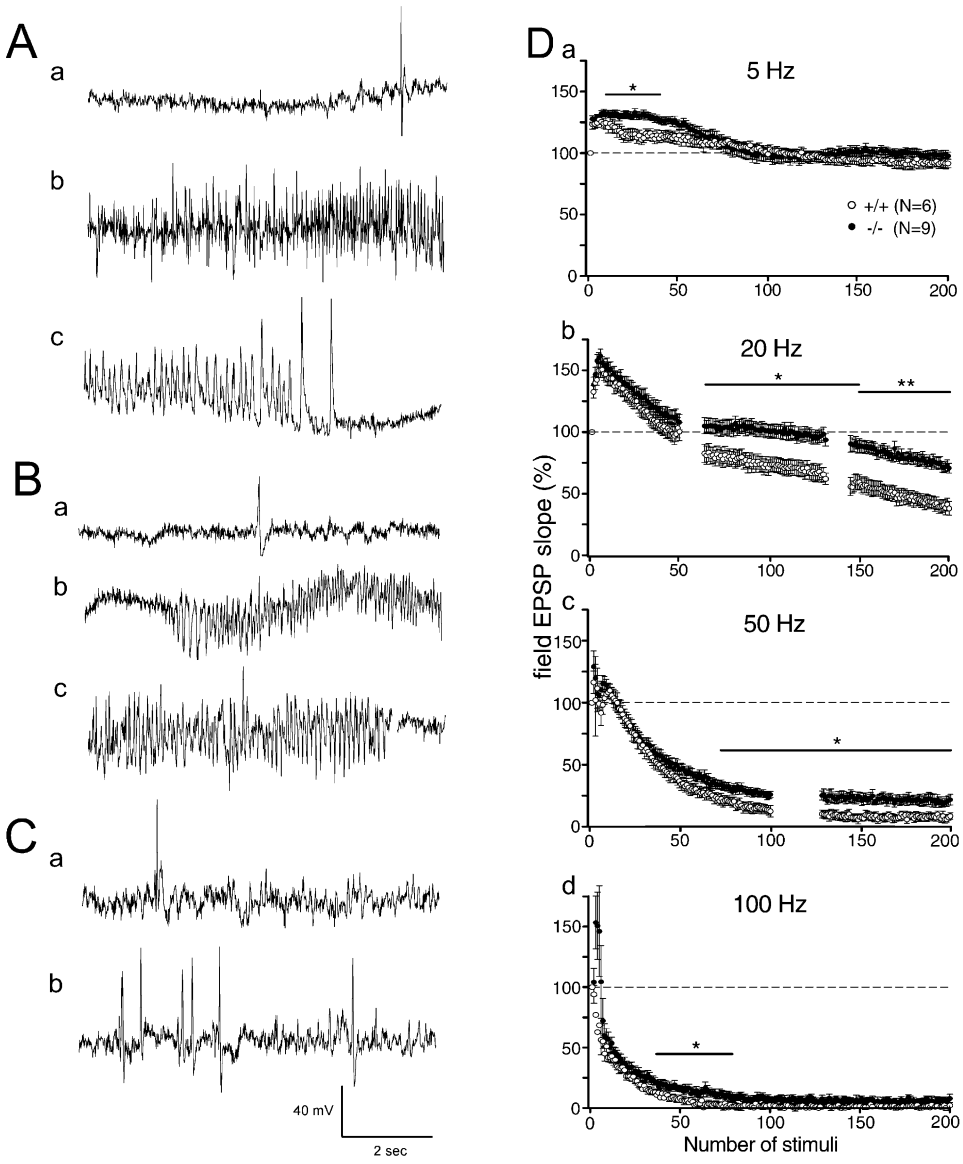

Figure 6. Assessment of the Epileptic Phenotype

EEG recordings from cortex (A) and hippocampus (B and C) of −/− mice. Regular EEG pattern interrupted by interictal spikes in the absence of seizures in cortex (Aa) and hippocampus (Ba). (Ab and Bb) Early phase of an electrographic seizure pattern, characterized by high-frequency spiking with increasing amplitude and synchronicity. This pattern is associated with behavioral seizures. (Ac and Bc) Late phase and end of an electrographic seizure pattern characterized by high-amplitude spiking at a reduced frequency and abrupt termination of paroxysmal activity, followed by low-amplitude EEG (postictal depression). (C) Hippocampal EEG of a mutant mouse before (Ca) and after (Cb) administration of MK-801. MK-801 markedly increased the frequency of spikes in the hippocampal EEG (Cb). (D) Response of fEPSPs (measured in the presence of 100 μM picrotoxin) to trains of 200 stimuli applied at frequencies of 5, 20, 50, and 100 Hz. The gaps in the 20 and 50 Hz plots are due to technical constraints. Note that −/− mutants displayed a stronger augmentation at 5 Hz and a smaller depression at higher frequencies (*$p < 0.05$; **$p < 0.01$; Mann-Whitney U test).

Analysis of the Epileptic Phenotype

As *Bsn* mutant mice develop pronounced seizures, we performed continuous video monitoring and EEG recording to assess the seizure phenotype in more detail. Spontaneous seizures with a frequency of up to four events per day were exclusively observed in homozygous mutants. They showed a typical pattern, with loss of righting reflex and generalized clonic convulsions with the mice lying on their side, followed by rearing and bilateral forelimb clonus. Duration of this convulsive activity varied between 18 and 33 s and was followed by a postictal immobility phase of 30–60 s. In part, mouth clonus was observed after termination of generalized seizure activity. In some −/− mice, myoclonic seizures were observed independently of generalized clonic seizures.

In the cortical and hippocampal EEG, behavioral seizures were paralleled by paroxysmal activity, characterized by high-frequency spiking (up to 24 Hz), increasing in amplitude and synchronicity during the seizure (Fig-

ures 6Ab and 6Bb). Toward the end of the paroxysmal activity, a transition to a pattern with lower frequency (7–8 Hz) but still high amplitude was observed. Between the seizures, single or accumulated high-amplitude interictal spikes occurred in EEG recordings of −/− mice (Figures 6Aa, 6Ba, and 6Ca), which were never observed in WT mice. In particular in the hippocampus, the frequency of interictal spikes was markedly increased on days on which seizures occurred.

As our functional studies indicated a reduced excitability of hippocampal principal neurons in *Bsn* mutant mice, we evaluated the consequences of pharmacological blockade of glutamate receptors in these mice by administration of a low, nontoxic dose of the NMDA antagonist MK-801. The mutants were strikingly more sensitive to motor impairment induced by MK-801 than WT controls. Cumulative scores for ataxia were 23.3 ± 1.3 in −/− (mean ± SEM, $n = 6$) compared to 8.3 ± 0.8 in WT mice ($n = 6$; $p < 0.05$). Most mutants exhibited a reduced righting reflex after MK-801, which was not observed in WT mice. Two mutant mice developed severe seizures after MK-801, whereas no seizures were seen in WT littermates. In the hippocampal and cortical EEG, all mutant mice showed paroxysmal spiking after MK-801 (Figure 6Cb). Compared to the average basal frequency of interictal spiking, a >7-fold increase in spike frequency was seen on average after MK-801. No such increase in spiking was seen in mutant mice after i.p. administration of saline, and no epileptiform spiking was observed after MK-801 in WT mice.

We further analyzed whether a dysregulation of glutamatergic synapses could contribute to the epileptic phenotype. The analysis of hippocampal CA1 synapses indicated a change in synaptic fatigue during trains of low-frequency stimulation in mutant as compared to WT mice (Figure 3C). Therefore we examined whether long-term stimulation at various frequencies differentially affects mutant and WT hippocampal synapses. Trains of 200 impulses were applied at a frequency of 5, 20, 50, and 100 Hz (Figures 6Da–6Dd). Five-Hz stimulation resulted in an augmentation that after ten stimuli became significantly more robust in −/− than in WT littermates (Figure 6Da). The augmentation decayed in both genotypes after 70 to 80 stimuli, but the responses did not fall below baseline level. When the same number of stimuli was given at 20, 50, or 100 Hz, a marked decline of responses was observed, the extent of which was positively correlated to the frequency applied (Figures 6Db–6Dd). In agreement with the slower decline of mutant responses during LFS for several minutes (Figure 3C), the decay of responses was significantly smaller in −/− than in WT animals. The difference was most pronounced at 20 Hz, where *Bsn* mutants were significantly less depressed for the last 120 responses of the train. The decay curves after trains at 50 Hz and 100 Hz could be well fitted by a one phase exponential decline yielding decay time constants (τ) of 0.31 s (+/+) versus 0.31 s (−/−) and 0.20 s (+/+) versus 0.27 s (−/−), respectively.

Discussion

The analysis of a mouse mutant lacking the central part of Bassoon demonstrates that this vertebrate-specific CAZ protein has essential functions at CNS synapses. In particular, we find that the loss of functional Bassoon causes a reduction in normal synaptic transmission, which can be attributed to the inactivation of a significant fraction of excitatory synapses. At these synapses, SVs are clustered and docked in normal numbers; however, they cannot fuse. The remaining active synapses are mostly normal with regard to quantal size, vesicular or synaptic release probabilities, vesicular refilling kinetics, or short-term plasticity. This reduction in normal synaptic transmission seen in dissociated neuronal cultures and slice preparations correlates well with the dramatic effects at the organismal level, i.e., epilepsy with rapidly generalizing seizures. Physiologically, the loss of Bassoon causes a unique set of synaptic changes that are not seen in other knockouts of genes encoding CAZ proteins.

Is *Bsn*$^{\Delta Ex4/5}$ a Hypomorphic Mutation?

The biochemical and cellular studies on the *Bsn* mutant mice indicate that deleting the central portion creates a mutation in Bassoon that prevents its anchoring to the CAZ. In particular, the cell fractionation experiments revealed that only about 10%–30% of BsnΔEx4/5 partitions into the synaptic protein fraction, as compared to almost 100% WT Bassoon. Furthermore, we find that very little BsnΔEx4/5 IR can be detected at synapses and that what is found there can be mostly extracted with methanol. These observations are consistent with data obtained when expressing deletion constructs of GFP-labeled Bassoon in primary hippocampal neurons (Dresbach et al., 2003) and demonstrate that the central region of Bassoon contains essential determinants for the integration of Bassoon into the synaptic cytomatrix. These findings have important implications for the interpretation of the mutant phenotype. Specifically, the lack of tight association of BsnΔEx4/5 with synaptic structures suggests that the observed mutant phenotype most likely is attributed to a loss of Bassoon function rather than a gain of function by mutated Bassoon. On the other hand, as accessory presynaptic targeting signals may reside in the N-terminal region of Bassoon (Dresbach et al., 2003), the residual protein may still be transported to synaptic nerve terminals—though less efficiently. Therefore, a dominant-negative effect of BsnΔEx4/5 cannot be completely ruled out. However, consistent with a loss-of-function effect of the *Bsn*$^{\Delta Ex4/5}$ mutation, we never observed epileptic seizures in heterozygous animals, suggesting that it is not the presence of BsnΔEx4/5 but the absence of WT Bassoon that is responsible for the epileptic phenotype.

Bassoon Is Required for Transmission at a Subset of Synapses

Electrophysiological analysis of synapse function in both hippocampal slices and in autaptic cultures revealed a 30%–50% reduced overall synaptic strength without changing short-term plasticity. This was accompanied by an overall reduction of the number of fusion-competent SVs. Most importantly, Bassoon-deficient synapses that participate in release had identical synaptic release probability, indicating that these synapses were properly equipped with fusion-competent SVs and

that their release efficiency was identical to SVs from WT neurons. Since mEPSC size and postsynaptic responsiveness were also unchanged, the most plausible explanation is that fewer synapses are release competent in the absence of WT Bassoon. Indeed, a quantitative analysis of synapse density combined with a functional comparison of SV cycling sites in autaptic cultures indicated that the same number of synapses are formed in the mutants, but about twice as many synapses are functionally silent. Other parameters that may account for synaptic strength did not show significant changes.

Consistent with the observations in situ, number, density, and protein composition of synapses appear unaltered in autaptic cultures, suggesting that these cultures mirror the in vivo situation. At the ultrastructural level, no obvious difference could be observed between active and inactive synapses—in particular, neither the density of SV clusters at the active zone nor the number of docked SVs differs significantly.

These observations indicate that the *Bsn* phenotype is unique in its degree but is comparable to a phenotype that was detected in mice deficient of another CAZ protein, Munc13-1 (Augustin et al., 1999). About 90% of excitatory synapses in hippocampal autapses rely on the SV priming capacity of Munc13-1, and its removal silenced these synapses yet did not alter the overall synaptic density or synaptic ultrastructure. In this respect, their phenotype is also comparable to that of synapses in Munc18 mutants (Verhage et al., 2000) or Munc13-1/Munc13-2 double mutants (Rosenmund et al., 2002), which also appear ultrastructurally normal but are completely inactive.

Intriguingly, inactivation upon removal of WT Bassoon concerns a fraction of synapses within a given excitatory neuron, as suggested by the analysis of microisland cultures and intracellular recordings of CA1 hippocampal neurons. The mechanism of how a reasonable fraction of the glutamatergic synapses of a single neuron become inactive whereas the remainder of the synapses are mostly normal in *Bsn* mutant mice is currently unclear. Double-immunolabeling experiments revealed that in WT autaptic cultures about 90% of Bassoon-positive synapses also contain Piccolo and vice versa. Since with any two antibodies against general synaptic marker proteins that we have tested the overlap was about 90%, we can assume that about 10% of synapses may escape immunodetection. Thus, Bassoon and Piccolo may be present in virtually all excitatory synapses in this culture system. Thus, silencing of "Bassoon-only" synapses cannot account for the fraction of inactive synapses. A possible explanation may be that the content of Bassoon and Piccolo has to reach a certain level for a synapse to be active. The 1.4-fold upregulation of Piccolo may ensure that this level is reached at a major fraction but not in all synapses.

Alternatively, as suggested in earlier studies, Bassoon may be involved in the proper assembly of the CAZ (Zhai et al., 2001), and its absence may cause stochastic failures in assembly. Although unlikely, we also cannot fully exclude the possibility that the residual BsnΔEx4/5 protein has still the propensity to fulfill Bassoon's function or has dominant-negative effects on synaptic function. In the former scenario, BsnΔEx4/5 may not reach all synapses in sufficient amounts due to its reduced targeting and/or anchoring efficiency, and synapses lacking BsnΔEx4/5 would be inactive. In the latter case, synapses that accumulate BsnΔEx4/5 would be perturbed in their function.

Finally, the phenotype could be due to microheterogeneity of the molecular composition of individual synapses within a neuron. Munc13-1 and Munc13-2 may serve as an example that this type of microheterogeneity exists (Rosenmund et al., 2002). Here, one may envision a scenario that Bassoon performs critical functions, e.g., in the recruitment of a priming factor, at some synapses and as in "Piccolo-only" synapses of the retina (Dick et al., 2001, 2003 [this issue of *Neuron*]) is not required for this function in other synapses. A comparison with mice mutant for Piccolo and analysis of double mutants may be required to fully elucidate the molecular function of these two proteins in assembly and function of the active zone.

Bsn Mutant Mice Have Recurring Epilepsy

The occurrence of epileptic seizures, as observed in $Bsn^{-/-}$ mutant mice, is frequently found associated with mutations in synaptic proteins, including synapsins and amphiphysins (Li et al., 1995; Di Paolo et al., 2002). It indicates a general imbalance of excitatory and inhibitory transmission. In $Bsn^{-/-}$ mutants, the systemic application of a low, nontoxic dose of MK-801 caused seizures and frequent epileptiform spiking in the hippocampus and cortex. One likely explanation for the proconvulsant effects of NMDA antagonists like MK-801 is the reduction of excitatory drive onto GABAergic interneurons and consequently a critical decrease of GABA release (Löscher, 1998; Löscher and Rogawski, 2002; Li et al., 2002). Therefore, the increased sensitivity to MK-801 of mutant as compared to WT mice may reflect a generally reduced glutamatergic transmission onto inhibitory interneurons in $-/-$ mutants.

Alternatively, an altered synaptic transmission between excitatory neurons may directly contribute to the epileptic phenotype. The stationary amplitude of individual EPSPs attained during trains of stimuli decreases if the stimulation frequencies exceed the limiting frequency, which lies between 10 and 25 Hz (Tsodyks and Markram, 1997). While mutant mice appear to have a lower number of active synapses than WT, they displayed a significantly reduced synaptic depression at frequencies above the limiting frequency. Notably, the paroxysmal discharges occurred in the same frequency range where the difference between mutant and WT mice attained its maximum ($\sim$20 Hz). Therefore, reduced synaptic fatigue at physiologically relevant firing rates may contribute to the generation and/or maintenance of epileptic seizures in *Bsn* mutants. Currently, it is unclear how this difference in synaptic depression during long trains of stimulation develops. One possibility would be that repetitive stimulation recruits inactive synapses in mutant slices. Another explanation may be that during ontogenesis the mutant brain has adapted to the reduced number of functional glutamatergic synapses, and the remainder synapses display an altered plasticity in response to longer lasting stimulation. More detailed studies on slice preparations and/or in vivo will have to address this issue.

In conclusion, our data suggest that Bassoon plays a pivotal role in the assembly and functioning of different types of synapses. While in the retina Bassoon turned out to be crucial for the functional assembly of photoreceptor ribbon synapses (Dick et al., 2003), in the hippocampus, deletion of functional Bassoon led to a lower excitability, reduced synaptic fatigue, and the silencing of a significant fraction of excitatory synapses. At the organismal level, these changes are likely to result in an impaired temporal coding of neuronal networks and in an enhanced propensity to undergo epileptic seizures.

Experimental Procedures

Gene Targeting and Production of *Bsn* Mutant Mice

A *lacZ/neo* cassette with an internal ribosome entry site for the *lacZ* transcript and a PGK promoter for the *neo* cassette was cloned into exon 4 and intron 5 of Bsn genomic DNA to replace half of exon 4 and the entire 6.6 kb of exon 5 (Figure 1A). Gene targeting and generation of the mouse line was performed as described (Talts et al., 1999).

Transcript Analysis

Northern blots from 20 μg of total RNA were analyzed with a cDNA probe from exon 2. To confirm the existence of ΔEx4/5 transcripts, the 200 bp PCR product resulting from nested RT-PCR with random primed cDNA (PCR primer pairs: CACCATGGGCAACGAGGCCAG CCT/GCTGGTTGAGCTCGCTGTCAGACA and CAAGCCAAAGACC ATGCCGAAGGA/TTCACCTTGCGGACCAGGCCGTTG) was subcloned and sequenced.

Antibodies

The following antibodies were used: Bassoon (Sap7f, tom Dieck et al., 1998), MAP2 (Sigma or Chemicon), panMunc13, RIM (Transduction Laboratories), synaptophysin, NR1 NMDA receptor, Synaptobrevin2 (Synaptic Systems), guinea pig or rabbit anti-Piccolo (Dick et al., 2001), anti-ProSAP1 (Boeckers et al., 1999). New antibodies were generated against N-terminal regions of Bassoon. Rabbit antiserum BSN5.3 was produced against the KLH-coupled peptide SRTQRSGRSPSVSPD (aa 130–144). Rabbit antiserum BSN6.3 was directed against a His-tagged fusion protein including aa 95–210 of Bassoon. Antibodies were affinity purified with a GST-fusion protein. Secondary antibodies for light microscopy were conjugated to Alexa Fluor 647, 546, 488 (Molecular Probes) or FITC (ICN Biomedicals).

Subcellular Protein Fractions

Cell fractionation was performed as described (Wyneken et al., 2001) with minor modifications. Briefly, brain homogenates were spun at 1000 × *g* for 10 min. The supernatant (S1) was centrifuged at 12,000 × *g* for 20 min, and the pellets were washed once. Supernatants were combined (S2). Pellets (P2) were further fractionated on a 0.85/1.0/1.2 M sucrose step gradient. The synaptosomal fraction (between 1.0 and 1.2 M sucrose) was hypotonically lysed and spun for 30 min at 33,000 × *g* to yield S3 (synaptosomal cytoplasm) and P3 (synaptosomal membranes). The latter were resuspended and further fractionated on a sucrose step gradient to obtain the synaptic junctional membrane fraction. Aliquots from each fraction were TCA precipitated, and 10 μg protein per fraction was separated on Tris acetate-buffered (125 mM, pH 7.0) 3.5%–8% polyacrylamide gradient gels and blotted onto PVDF membrane (Millipore). For blotting, the NuPAGE™ system protocol (Invitrogen) with modifications in the running buffer (addition of 1 mM glutathion) and transfer buffer (addition of 5% methanol) was used. Immunodetection was performed with the ECL system (Amersham). Films were digitized, and intensities of immunosignals were quantified using the Quantity One Software (Biorad).

Immunofluorescence Microscopy of Primary Hippocampal Cultures

Hippocampal cultures were prepared individually from single newborn mice as turn-over cultures and grown on coverslips (Brewer and Cotman, 1989). Cells were fixed at 14 div with methanol or 4% formaldeyde. For immunofluorescence analysis, samples were quenched (15 min, 25 mM glycine), blocked (1 hr; 2% BSA, 10% horse serum, 0.3% Triton X-100 in PBS), and incubated with primary antibodies followed by appropriate secondary antibodies in block solution. Images were obtained on a Leica microscope with a CCD camera (Visitron Systems) and processed with Photoshop (Adobe Systems).

Ultrastructural Analysis of Brain Sections

Anaesthetized male mice were perfused transcardially with 0.9% NaCl (1 min) followed by a fixative (2% glutaraldehyde, 2% formaldehyde for conventional EM; 4% formaldehyde, 0.05% glutaraldehyde, 0.18% picric acid for immuno-EM) for 15 min. Brains were removed and vibratome sectioned. For conventional electron microscopy (EM), 200 μm vibratome slices were fixed for 60 min in 1% OsO_4 in 0.1 M cacodylate buffer, dehydrated in a graded ethanol series including a 45 min block staining with 2% uranyl acetate in 70% ethanol, and flat embedded in Durcupan. Thin silver sections were stained with uranyl acetate and lead citrate and examined on a Zeiss EM 900. For immuno-EM, pieces of 500 μm vibratome sections were infused with 2.3 M sucrose (>2 hr), frozen in liquid nitrogen, and cut on a cryo-ultramicrotome (Leica). Ultrathin sections were mounted on formvar-coated nickel grids and immunolabeled (Griffiths, 1993) using first rabbit anti-Piccolo antiserum (1:100) and 10 nm gold-labeled goat-anti-rabbit secondary antibody (British Biocell). Thereafter, grids were embedded and contrasted in a mixture of methylcellulose and uranyl acetate.

Slice Electrophysiology

Hippocampal transverse slices (400 μm) were maintained for 1 hr at 32°C in oxygenated artificial cerebrospinal fluid (ACSF), transferred to a recording chamber, and continuously superfused with ACSF (2.5 ml/min). To record fEPSPs, a Pt-Ir stimulation electrode and a glass recording electrode (filled with ACSF, 1–4 MΩ) were placed in the CA1 stratum radiatum. Pharmacologically separated EPSCs and IPSCs were recorded in whole-cell configuration with glass pipettes (5 MΩ) filled with a solution containing (in mM) K-gluconate, 135; $MgCl_2$, 5; HEPES, 10; glucose, 20; pH 7.2. EPSCs were separated by using Picrotoxin (Sigma-Aldrich) (100 μM), IPSCs by means of CNQX (6-Cyano-7-nitroquinoxaline-2,3-dione; 10 μM) supplemented with either CPP [3-(R-2-Carboxypiperazin-4yl)-propyl-1-phosphonic acid; 10 μM] or AP5 (D-2Amino-5-phosphonopentanoic acid; 50 μm) (Tocris). EPSCs were recorded at a holding potential of −65mV, IPSCs at −50mV. Recordings were conducted with a patch-clamp amplifier (Axoclamp2A or Axopatch200B, Axon Instruments). The responses were filtered at 1 kHz, digitized at 5 kHz. Statistical analysis was performed using the two-tailed Mann-Whitney U test and ANOVA for evaluating between groups.

Culture, Electrophysiology, and FM1-43 Imaging of Autaptic Hippocampal Cultures

Primary microisland cultures were prepared from newborn littermates from $Bsn^{+/-}$ parents, and recordings were performed as described (Fernández-Chacón et al., 2002; Rosenmund et al., 2002). Measurements are presented as mean ± standard error. Statistical significance between two groups was estimated using the unpaired nonparametric Student's t test. FM1-43 staining and destaining experiments were performed as described in Rosenmund et al., 2002. Here, synapses were FM stained by a 1 s application of a solution containing 150 mM KCl and were destained with 15 s of 75 mM KCl. Afterward, cells were fixed in 4% formaldehyde and immunostained for synaptophysin, Piccolo, and MAP2. Images from FM1-43 cycling and immunostains were Laplace filtered with TILLvisION 4.0 (TILL Photonics) and merged with Photoshop (Adobe). The degree of colocalization was determined manually.

For double or triple immunostainings for Synaptophysin, Piccolo, NR1, or Synaptobrevin2/VAMP2, ProSAP1 and Piccolo cells were formaldehyde or methanol fixed, and images were processed and analyzed in Photoshop essentially as described previously (Dick et al., 2001).

EEG and Video Recordings of Seizures and Pharmacological Experiments

For EEG recordings, stainless-steel electrodes were stereotaxically implanted into the right hippocampus and bilaterally over the cortex in anesthetized mice using stereotaxic coordinates derived from Paxinos and Franklin (2000). Hippocampal and cortical EEG recordings were started after a postsurgery recovery period of at least 3 days in conscious mice that were connected via a flexible and shielded cable and a swivel to an EEG recording system. In parallel to the EEG recordings, the animals were video monitored during the light phase for 8 hr per day, up to a total of 40 hr. All video and EEG recordings were viewed for paroxysmal activity or other signs of neurological abnormalities. Following the experiments, the correct location of hippocampal electrodes was histologically verified (Gernert et al., 2000).

For pharmacological manipulation of glutamatergic neurons, behavior and EEG were recorded before and for up to 4 hr after injection of the NMDA antagonist MK-801. Behavioral alterations induced by MK-801 were scored after 15, 30, 60, 90, 120, and 240 min by a grading system described previously (Wlaz et al., 1994), and cumulative scores were used for statistical group comparisons. Furthermore, paroxysmal EEG alterations were quantified before and after MK-801.

All animal experiments were performed in compliance with the guidelines for the welfare of experimental animals issued by the Federal Government of Germany, the National Institutes of Health, and the Max Planck Society.

Acknowledgments

This paper is dedicated to Kathrin Zobel, the most outstanding technician, who unexpectedly died while this work was in progress. We are grateful to K. Zobel, K. Hartung, B. Kracht, K. Schumacher, A. Hildebrand, I. Herfort, G.-S. Nam, and A. Rudloff for expert technical assistance; to F. Schmitz for advice on the quantification of EM data; J.L. Noebels for discussion of the epileptic phenotype; and O. Dick, B. Qualmann, J. Montgomery, and M. Kessels for many helpful discussions. This work was supported by the DFG SFB426 to E.D.G., J.U.F., S.t.D., and D.B.; SFB269 and Heisenberg Fellowships to J.H.B. and C.R.; the Fonds der Chemischen Industrie to E.D.G.; INTAS (Ref.-No. 97-10090) to J.U.F.; the Boehringer Ingelheim Fonds to A.C.M.; and the NIH (RO1 NS39471; PO1 AG06569; P50 HD32901) to C.C.G.

Received: November 16, 2001
Revised: December 19, 2002

References

Augustin, I., Rosenmund, C., Südhof, T.C., and Brose, N. (1999). Munc13-1 is essential for fusion competence of glutamatergic synaptic vesicles. Nature *400*, 457–461.

Betz, A., Thakur, P., Junge, H.J., Ashery, U., Rhee, J.S., Scheuss, V., Rosenmund, C., Rettig, J., and Brose, N. (2001). Functional interaction of the active zone proteins Munc13-1 and RIM1 in synaptic vesicle priming. Neuron *30*, 183–196.

Boeckers, T.M., Kreutz, M.R., Winter, C., Zuschratter, W., Smalla, K.-H., Sanmarti-Vila, L., Wex, H., Langnaese, K., Bockmann, J., Garner, C.C., and Gundelfinger, E.D. (1999). Proline-rich synapse-associated protein-1/cortactin binding protein 1 (ProSAP1/CortBP1) is a PDZ-domain protein highly enriched in the postsynaptic density. J. Neurosci. *19*, 6506–6518.

Brandstätter, J.H., Fletcher, E.L., Garner, C.C., Gundelfinger, E.D., and Wassle, H. (1999). Differential expression of the presynaptic cytomatrix protein bassoon among ribbon synapses in the mammalian retina. Eur. J. Neurosci. *11*, 3683–3693.

Brewer, G.J., and Cotman, C.W. (1989). Survival and groWTh of hippocampal neurons in defined medium at low density: advantages of a sandwich culture technique or low oxygen. Brain Res. *494*, 65–74.

Brodin, L., Low, P., Gad, H., Gustafsson, J., Pieribone, V.A., and Shupliakov, O. (1997). Sustained neurotransmitter release: new molecular clues. Eur. J. Neurosci. *9*, 2503–2511.

Di Paolo, G., Sankaranarayanan, S., Wenk, M.R., Daniell, L., Perucco, E., Caldarone, B.J., Flavell, R., Picciotto, M.R., Ryan, T.A., Cremona, O., and De Camilli, P. (2002). Decreased synaptic vesicle recycling efficiency and cognitive deficits in amphiphysin 1 knockout mice. Neuron *33*, 789–804.

Dick, O., Hack, I., Altrock, W.D., Garner, C.C., Gundelfinger, E.D., and Brandstatter, J.H. (2001). Localization of the presynaptic cytomatrix protein Piccolo at ribbon and conventional synapses in the rat retina: Comparison with Bassoon. J. Comp. Neurol. *439*, 224–234.

Dick, O., tom Dieck, S., Altrock, W.D., Ammermüller, J., Weiler, R., Garner, C.C., Gundelfinger, E.D., and Brandstätter, J.H. (2003). The presynaptic active zone protein Bassoon is essential for photoreceptor ribbon synapse formation in the retina. Neuron *37*, this issue, 775–786.

Dresbach, T., Qualmann, B., Kessels, M.M., Garner, C.C., and Gundelfinger, E.D. (2001). The presynaptic cytomatrix of brain synapses. Cell. Mol. Life Sci. *58*, 94–116.

Dresbach, T., Hempelmann, A., Spilker, C., tom Dieck, S., Altrock, W.D., Zuschratter, W., Garner, C.C., and Gundelfinger, E.D. (2003). Functional regions of the presynaptic cytomatrix protein Bassoon: significance for synaptic targeting and cytomatrix anchoring. Mol. Cell. Neurosci., in press.

Fenster, S.D., Chung, W.J., Zhai, R., Cases-Langhoff, C., Voss, B., Garner, A.M., Kampf, U., Kindler, S., Gundelfinger, E.D., and Garner, C.C. (2000). Piccolo, a presynaptic zinc finger protein structurally related to Bassoon. Neuron *25*, 203–214.

Fernández-Chacón, R., Shin, O.K., Königstorfer, A., Matos, M.F., Meyer, A.C., Garcia, J., Gerber, S.H., Rizo, J., Südhof, T.C., and Rosenmund, C. (2002). Structure/function analysis of Ca2+-binding to the C2A-domain of synaptotagmin 1. J. Neurosci. *22*, 8438–8446.

Garner, C.C., Zhai, R.G., Gundelfinger, E.D., and Ziv, N.E. (2002). Molecular mechanisms of CNS synaptogenesis. Trends Neurosci. *25*, 243–251.

Gernert, M., Bloms-Funke, P., Ebert, U., and, Loscher, W. (2000). Kindling causes persistent in vivo changes in firing rates and glutamate sensitivity of central piriform cortex neurons in rats. Neurosci. *99*, 217–227.

Griffiths, G. (1993). Fine Structure Immunocytochemistry (Berlin: Springer).

Li, L., Chin, L.S., Shupliakov, O., Brodin, L., Sihra, T.S., Hvalby, O., Jensen, V., Zheng, D., McNamara, J.O., Greengard, P., and Andersen, P. (1995). Impairment of synaptic vesicle clustering and of synaptic transmission, and increased seizure propensity, in synapsin I-deficient mice. Proc. Natl. Acad. Sci. USA *92*, 9235–9239.

Li, Q., Clark, S., Lewis, D.V., and Wilson, W.A. (2002). NMDA receptor antagonists disinhibit rat posterior cingulate and retrosplenial cortices: a potential mechanism of neurotoxicity. J. Neurosci. *22*, 3070–3080.

Löscher, W. (1998). Pharmacology of glutamate receptor antagonists in the kindling model of epilepsy. Prog. Neurobiol. *54*, 721–741.

Löscher, W., and Rogawski, M.A. (2002). Epilepsy. In Ionotropic Glutamate Receptors as Therapeutic Targets, D. Lodge, W. Danysz, and C.G. Parsons, eds. (Johnson City, TN: Graham Publ.) pp.91–132.

Ohtsuka, T., Takao-Rikitsu, E., Inoue, E., Inoue, M., Takeuchi, M., Matsubara, K., Deguchi-Tawarada, M., Satoh, K., Morimoto, K., Nakanishi, H., and Takai, Y. (2002). CAST: a novel protein of the cytomatrix at the active zone of synapses that forms a ternary complex with RIM1 and Munc13-1. J. Cell Biol. *158*, 577–590.

Paxinos, G., and Franklin, K.B.J. (2000). The Mouse Brain in Stereotaxic Coordinates, Second Edition (Sydney: Academic Press).

Peters, A., Palay, S.L., and Webster, H. (1991). Synapses. In The Fine Structure of the Nervous System. Neurons and Their Supporting Cells, Third Edition (Cambridge: Oxford University Press), pp.138–211.

Rhee, J.S., Betz, A., Pyott, S., Reim, K., Varoqueaux, F., Augustin, I., Hesse, D., Sudhof, T.C., Takahashi, M., Rosenmund, C., and Brose, N. (2002). β-Phorbol ester- and diacylglycerol-induced aug-

mentation of transmitter release is mediated by Munc13s and not by PKCs. Cell *108*, 121–133.

Richter, K., Langnaese, K., Kreutz, M.R., Olias, G., Zhai, R., Scheich, H., Garner, C.C., and Gundelfinger, E.D. (1999). Presynaptic cytomatrix protein Bassoon is localized at both excitatory and inhibitory synapses of rat brain. J. Comp. Neurol. *408*, 437–448.

Rosenmund, C., and Stevens, C.F. (1996). Definition of the readily releasable pool of vesicles at hippocampal synapses. Neuron *16*, 1197–1207.

Rosenmund, C., Clements, J.D., and Westbrook, G.L. (1993). Nonuniform probability of glutamate release at a hippocampal synapse. Science *262*, 754–757.

Rosenmund, C., Sigler, A., Augustin, I., Reim, K., Brose, N., and Rhee, J.S. (2002). Differential control of vesicle priming and short-term plasticity by Munc13 isoforms. Neuron *33*, 411–424.

Schoch, S., Castillo, P.E., Jo, T., Mukherjee, K., Geppert, M., Wang, Y., Schmitz, F., Malenka, R.C., and Sudhof, T.C. (2002). RIM1α forms a protein scaffold for regulating neurotransmitter release at the active zone. Nature *415*, 321–326.

Südhof, T.C. (1995). The synaptic vesicle cycle: a cascade of protein-protein interactions. Nature *375*, 645–653.

Südhof, T.C. (2000). The synaptic vesicle cycle revisited. Neuron *28*, 317–320.

Talts, J.F., Brakebusch, C., and Fassler, R. (1999). Integrin gene targeting. Methods Mol. Biol. *129*, 153–187.

tom Dieck, S., Sanmarti-Vila, L., Langnaese, K., Richter, K., Kindler, S., Soyke, A., Wex, H., Smalla, K.-H., Kampf, U., Franzer, J.T., et al. (1998). Bassoon, a novel zinc-finger CAG/glutamine-repeat protein selectively localized at the active zone of presynaptic nerve terminals. J. Cell Biol. *142*, 499–509.

Tsodyks, M.V., and Markram, H. (1997). The neural code between neocortical pyramidal neurons depends on neurotransmitter release probability. Proc. Natl. Acad. Sci. USA *94*, 719–723.

Vardinon-Friedman, H., Bresler, T., Garner, C.C., and Ziv, N.E. (2000). Assembly of new individual excitatory synapses: time course and temporal order of synaptic molecule recruitment. Neuron *27*, 57–69.

Verhage, M., Maia, A.S., Plomp, J.J., Brussaard, A.B., Heeroma, J.H., Vermeer, H., Toonen, R.F., Hammer, R.E., van den Berg, T.K., Missler, M., et al. (2000). Synaptic assembly of the brain in the absence of neurotransmitter secretion. Science *287*, 864–869.

Wang, Y., Okamoto, M., Schmitz, F., Hofmann, K., and Sudhof, T.C. (1997). Rim is a putative Rab3 effector in regulating synaptic-vesicle fusion. Nature *388*, 593–598.

Wang, X., Kibschull, M., Laue, M.M., Lichte, B., Petrasch-Parwez, E., and Kilimann, M.W. (1999). Aczonin, a 550-kD putative scaffolding protein of presynaptic active zones, shares homology regions with Rim and Bassoon and binds profilin. J. Cell Biol. *147*, 151–162.

Wlaz, P., Ebert, U., and Loscher, W. (1994). Low doses of the glycine/NMDA receptor antagonist R-(+)-HA-966 but not D-cycloserine induce paroxysmal activity in limbic brain regions of kindled rats. Eur. J. Neurosci. *6*, 1710–1719.

Wyneken, U., Smalla, K.-H., Marengo, J.J., Soto, D., de la Cerda, A., Tischmeyer, W., Grimm, R., Boeckers, T.M., Wolf, G., Orrego, F., and Gundelfinger, E.D. (2001). Kainate-induced seizures alter protein composition and N-methyl-D-aspartate receptor function of rat forebrain postsynaptic densities. Neuroscience *102*, 65–74.

Zhai, R.G., Vardinon-Friedman, H., Cases-Langhoff, C., Becker, B., Gundelfinger, E.D., Ziv, N.E., and Garner, C.C. (2001). Assembling the presynaptic active zone: a characterization of an active one precursor vesicle. Neuron *29*, 131–143.

Zhang, L., Volknandt, W., Gundelfinger, E.D., and Zimmermann, H. (2000). A comparison of synaptic protein localization in hippocampal mossy fiber terminals and neurosecretory endings of the neurohypophysis using the cryo-immunogold technique. J. Neurocytol. *29*, 19–30.

Zucker, R.S. (1989). Short-term synaptic plasticity. Annu. Rev. Neurosci. *12*, 13–31.